CUPP-97/2
hep-ph/9708444

Next to Minimal Higgs : Mass Bounds and Search Prospects

Anindya Datta [1,♡], *Amitava Raychaudhuri* [2,†]
[1]Physics Department, Taki Government College,
Taki, North 24 Pgs. 743429, India.
[2]Department of Physics, University of Calcutta,
92 Acharya Prafulla Chandra Road, Calcutta 700009, India.

ABSTRACT

The Standard Model of electroweak interactions has one scalar doublet. The minimal extension of this sector is effected by adding a neutral, singlet scalar field. Depending on whether the singlet field has a non-zero vacuum expectation value, x, or not, the scenario has quite distinctive predictions. In particular, $x \neq 0$ produces a mixing between the usual $SU(2)$ doublet and the singlet, giving rise to two physical states and a goldstone boson with non-vanishing coupling to these. Presence of this coupling modifies the $2jets + \not{E}$ signal of the Bjorken process at LEP. We update the bounds on the Higgs mass using the LEP-1 data. We then explore, using parton-level Monte Carlo event generators, the production of these scalars at the LHC via gluon-gluon fusion and subsequent detection. We compare the signals with the expected backgrounds.

July 1997

Electronic addresses: ♡anindya@cubmb.ernet.in; †amitava@cubmb.ernet.in

1 INTRODUCTION

Perhaps the most challenging problem facing the particle physics community today is the observation and understanding of the Higgs boson, which plays the key role of breaking the $SU(2) \times U(1)$ symmetry of electroweak interactions. Efforts to find this elementary scalar have so far proved fruitless and the absence of the Bjorken process Higgs signal at LEP-1 sets a lower mass limit of 60.2 GeV [1, 2, 3].

Different extensions of the Higgs structure of the Standard Model (SM) have been examined in the literature [4]. Of these, the minimal is one where a neutral, $SU(2)$ singlet scalar field is included along with the doublet. Such singlets are common in superstring inspired models like E_6 [5], in composite models [6], in the next to minimal supersymmetric standard model [7], *etc.* The neutral singlet scalar, N, cannot directly interact with the standard quarks and leptons but couples to the SM doublet through quartic terms in the potential. In the event that N develops a vacuum expectation value (*vev*) the spontaneous breakdown of a global $U(1)$ symmetry is triggered off and a Goldstone mode, J, emerges. This boson is the 'Majoron' in models where lepton number is identified with the $U(1)$ symmetry [8]. Further, the real part of the singlet mixes with the neutral member of the doublet. Thus there are two physical scalars H_1 and H_2 both of which couple to the other members of the SM. They can be produced either at e^+e^- colliders by the Bjorken process or at a hadron collider by gluon-gluon fusion. Both have non-vanishing coupling to J, resulting in an enrichment of the decay modes. In particular, the decay $H_i \to JJ$ is an invisible mode which affects the usual analyses for Higgs scalar mass limits [9, 10].

In the present work, we first consider the situation where N has no vacuum expectation value. Even in this case, a quartic term in the scalar potential yields a coupling that drives the decay $H \to NN$. The resultant effect on the Higgs mass bound from LEP-1 is first investigated. Next we turn to the case where N has a non-zero *vev*. We update the mass bounds [11] on scalars in such a scenario using the LEP-1 results on Higgs search following the published data from the L3 group [1]. We then move on to the production and decay scenarios of the scalars of this model at hadron colliders. Their production through gluon-gluon fusion, though similar to that in the SM, carries an additional mixing angle suppression. Among the various decay modes, we emphasize the decay of the heavier scalar into a pair of the lighter variety and the subsequent decay of these into either $b\bar{b}$ or into Js thus resulting in $4b$ or $2b + \not{E}_T$ final states. The main SM backgrounds to these processes are, respectively, the hadronic $4b$ events and $2b + gluon$ final states where the gluon jet is outside the rapidity coverage of the detector, giving rise to missing E_T. We have estimated the signal and the SM backgrounds using parton-level Monte Carlo event generators.

The plan of this article is as follows. In section 2, we discuss the scalar potential of the

model and the resulting mass matrix. We also relate the parameters of the potential with the masses of the physical states and the mixing angle. In section 3, we begin with the case where N has no *vev* and in the next section incorporate a nonzero *vev* of N and update the bounds on the scalar masses using the LEP-1 data. In section 5, we turn to the LHC and examine the production rates and decay branching ratios of the scalars as well as their signals and possible backgrounds. The conclusions are in section 6.

2 THE SCALAR POTENTIAL AND THE RELEVANT COUPLINGS

The most general scalar potential, invariant under $SU(2) \times U(1)$, containing the doublet Φ and the neutral, singlet field N can be written as:

$$\mathcal{V} = \mu^2 \Phi^\dagger \Phi + m^2 N^* N + \lambda (\Phi^\dagger \Phi)^2 + \lambda' (N^* N)^2 + \xi \Phi^\dagger \Phi N^* N \tag{1}$$

The potential has an additional $U(1)$ symmetry corresponding to the phase of N. All the other particles are neutral under this $U(1)$. (In Majoron models, this symmetry is identified with lepton number.)

To start with, consider the case where the singlet field does not acquire any *vev*. $SU(2) \times U(1)$ symmetry forbids any coupling of N to the standard quarks, leptons and gauge bosons. It only interacts with the doublet scalar through the last term in eq. (1) which can result in the decay $H \to NN$, where H is the physical Higgs boson. The decay products for this mode will be invisible. We discuss the details in the next section.

Next, consider the situation where the *vev* of N is non-zero. Let $v/\sqrt{2}$ and $x/\sqrt{2}$ be the *vev*s – both chosen real – for the doublet and the singlet fields respectively. v is related to the W boson mass by the relation $m_W = \frac{1}{2} g v$. x breaks the $U(1)$ symmetry alluded to above and the imaginary part of N becomes a goldstone field J. The ratio $tan\beta = (x/v)$ will be a free parameter of our analysis. The quartic term $\xi \Phi^\dagger \Phi N^* N$ and the *vev* of the singlet scalar field generates a mixing between H_d and H_s, the real parts of the neutral component of Φ and N.

Minimisation of the scalar potential demands,

$$\mu^2 = -\lambda v^2 - \frac{1}{2}\xi x^2; \quad \text{and} \quad m^2 = -\lambda' x^2 - \frac{1}{2}\xi v^2 \tag{2}$$

The mass matrix of the real scalar fields is:

$$M^2 = \begin{pmatrix} 2\lambda v^2 & \xi x v \\ \xi x v & 2\lambda' x^2 \end{pmatrix} \tag{3}$$

The mass eigenstates H_1 and H_2 are written as:

$$H_1 = H_d \cos\ \theta + H_s \sin\ \theta; \quad \text{and} \quad H_2 = -H_d \sin\ \theta + H_s \cos\ \theta \tag{4}$$

where

$$\tan 2\theta = \frac{\xi x v}{\lambda v^2 - \lambda' x^2} \tag{5}$$

The remaining parameters of the scalar potential can be expressed in terms of the masses m_i of H_i, the mixing angle θ and $\tan\beta$:

$$\lambda = \frac{g^2}{8m_W^2}(m_1^2\ \cos^2\theta + m_2^2\ \sin^2\theta) \tag{6}$$

$$\lambda' = \frac{g^2}{8m_W^2 \tan^2\beta}(m_1^2\ \sin^2\theta + m_2^2\ \cos^2\theta) \tag{7}$$

$$\xi = \frac{g^2(m_1^2 - m_2^2)\sin 2\theta}{8\, m_W^2\ \tan\beta} \tag{8}$$

A check is applied to ensure that none of these couplings exceeds unity.
The couplings of the SM fermions with H_i are the same as the SM Higgs-fermion ones, save appropriate mixing angle factors. But in this model H_i also couples to a pair of H_j $(i, j = 1, 2;\ i \neq j)$ and to the Js. As these are of particular relevance, we write them here explicitly.

$$\mathcal{L}_{H_1 JJ} = -(\lambda^{'} x \sin\theta + \frac{1}{2}\xi v \cos\theta) H_1 JJ \tag{9}$$

$$\mathcal{L}_{H_2 JJ} = -(\lambda^{'} x \cos\theta - \frac{1}{2}\xi v \sin\theta) H_2 JJ \tag{10}$$

$$\begin{aligned}\mathcal{L}_{H_1H_2H_2} &= -\Big[3\ \cos\theta\ \sin^2\theta\, v\, \lambda + 3\ \cos^2\theta\ \sin\theta\, x\, \lambda' + \frac{1}{2}\cos^3\theta\, v\, \xi \\ &\quad -\ \cos\theta\ \sin^2\theta\, v\, \xi -\ \cos^2\theta\ \sin\theta\, x\, \xi + \frac{1}{2}\sin^3\theta\, x\, \xi\Big]\, H_1 H_2 H_2\end{aligned} \tag{11}$$

$$\begin{aligned}\mathcal{L}_{H_2H_1H_1} &= -\Big[-3\ \sin\theta\ \cos^2\theta\, v\, \lambda + 3\ \sin^2\theta\ \cos\theta\, x\, \lambda' - \frac{1}{2}\sin^3\theta\, v\, \xi \\ &\quad +\ \sin\theta\ \cos^2\theta\, v\, \xi -\ \sin^2\theta\ \cos\theta\, x\, \xi + \frac{1}{2}\cos^3\theta\, x\, \xi\Big]\, H_2 H_1 H_1\end{aligned} \tag{12}$$

3 MASS BOUND FROM LEP-1: $x = 0$ CASE

As noted in the previous section, if the *vev* of N is zero then its only interaction is with the Φ through a quartic term in the potential – see eq. (1). If H is the physical Higgs field after spontaneous breakdown of the $SU(2) \times U(1)$ symmetry then the above coupling drives the decay of H to a pair of Ns, if kinematically allowed. (It needs to be borne in mind that N is a *complex* neutral field.) The singlet scalar cannot couple to the quarks, leptons, and gauge bosons. Thus Higgs decay in this channel leaves no signature in the detector and can only be surmised from the momentum imbalance of the final state particles. At an e^+e^- collider, when the doublet Higgs is produced along with an off-shell Z-boson by the Bjorken process, only the decay products of the latter will be seen in the detector. In particular, a hadronic Z-decay produces a final state with two jets and missing energy from the Higgs decay which mimics the SM process where the Z decays invisibly (*i.e.* to neutrinos) while the Higgs decays hadronically. With this additional mode in the picture, the bound on the Higgs mass from the LEP-1 data is modified. The L3 collaboration [1] has searched for the di-jet $+ \not{E}$ signature in a data sample of 3.05 million hadronic Z decays and from its absence has imposed a 95% C.L. lower limit of 60.2 GeV [1] on the SM Higgs mass. We can translate this bound for the case under discussion by incorporating in the analysis the additional $H \to NN$ decay mode. Instead of using a detailed Monte Carlo event generator and applying the appropriate cuts used by the L3 group, we demand that:

$$[\Gamma(Z \to \nu\bar{\nu}H)B.R.(H \to b\bar{b}, c\bar{c})\epsilon_{vis} + \Gamma(Z \to (q\bar{q})H)B.R.(H \to NN)\epsilon_{invis}] < 3\Gamma(Z \to hadrons)/3.05 \times 10^6 \quad (13)$$

In the above, the ϵs are the efficiencies of the topological cuts used by L3 to differentiate between the signal and the background. Since no excess over background has been observed, the 95% C.L. limit corresponds to a signal of 3 events. The Z-bosons produced at LEP-1 are predominantly transverse and in the derivation of $\Gamma(Z \to \nu\bar{\nu}H)$ or $\Gamma(Z \to b\bar{b}H)$ we sum over only these polarisation states of the parent Z.
We present our results in fig. 1 for three representative values of the quartic coupling constant ξ, namely, $\xi = 1$ (solid curve), .0001 (large-dashed curve), and 0 (small-dashed curve), and $m_N = 20$ (1a) and 0 (1b) GeV. Of course, in the above, $\xi = 0$ is just the SM limit. The lower bound on m_H from eq. (13) corresponds to the point of intersection of the curves with the abscissa. From the figure it is seen that this limit is almost insensitive to m_N and increases with the increase of ξ, with $m_H > 66.0$ GeV for $\xi = 1$, reducing to the SM value in the $\xi = 0$ limit. The curves for all values of ξ in the range 1 to 0.01 are practically coincident since for these cases the branching ratio for $H \to NN$ is essentially unity. Only when ξ gets smaller, do the other modes

become comparable. (The L3 group also briefly discusses the search for an invisibly decaying Higgs particle without going into details of any particular model [1], and a 95% C.L. lower limit on the mass of such a scalar is quoted as 66.7 GeV – similar to the one in the $\xi = 1$ case.)

At this point it will be meaningful to compare the branching ratio in this model of some decay channel (any channel important in the context of SM Higgs search) with that in the Standard Model. As an example, the ratio of the corresponding BR's for the case of $\gamma\gamma$ decay is presented in fig. 2 as a function of m_H for different values of the parameter ξ. Though the partial width for $H \to \gamma\gamma$ is unchanged in this case, the total width has an additional contribution from $H \to NN$. The exhibited ratio is thus just $\Gamma(H)_{SM}/\Gamma(H)$.

4 MASS BOUND FROM LEP-1: $x \neq 0$ CASE

As already noted in section 2, when the singlet scalar has a nonzero *vev* there are two physical massive scalar fields H_1 and H_2 and a Goldstone boson, J. If one or both of the H_i are lighter than the Z then they will be produced *via* the Bjorken process at LEP-1 so that the data can be used to set a bound on their masses. For small values of $\tan\beta$, both have considerable decay branching ratios to a pair of Js, an invisible decay mode. Thus, once produced by the Bjorken process, they can give rise to much the same signal as discussed in the previous section, decaying into a pair of Js, and with the Z^{0*} decaying to a $q\bar{q}$ pair, mimicing the di-jet + $\not{E}$ signal of a Higgs scalar. As in the previous section, to derive the lower bounds on the scalar masses we require that the constraint of eq. (13) be satisfied. Of course, in this case the left side of the equation depends on m_1, m_2, θ and $\tan\beta$. As already noted, there are two possibilities: (a) when both $m_1,\ m_2 < m_Z$ and (b) when only one of the scalars is lighter than the Z and contributes.

We let the mixing angle θ vary from 0 to $\pi/2$. It is readily seen that the range $\pi/2 \leq \theta \leq \pi$ can be mapped to the previous one by the redefinition of $H_1 \to H_2$ and $H_2 \to -H_1$ – see eq. (4).

The situation dealt with in the previous section corresponds to $\tan\beta = 0$. Here we let it vary in the range $1 \leq \tan\beta \leq 10$ which corresponds to a maximum value of $x \simeq 2$ TeV.

We present in fig. 3 our results for the case where both scalars are lighter than m_Z for two representative values of $\tan\beta$, namely 1 (solid line), and 10 (dashed line). Three choices of the mixing angle – *viz.* $\theta = 5^o$, 45^o, and 85^o – are considered. The allowed masses lie in the region to the right of the curves. From the figure it is seen that the lower mass limit can be substantially low for small or large values of the mixing angle

θ. On the contrary, for the case $\theta = 45^o$ both scalars are heavier than about 55 GeV. We have not exhibited the region below a mass of 20 GeV. In fact, a small window survives in the mass range of 5 – 10 GeV. This is an artefact of the low efficiency of detection for this mass range.

If one of the scalars has a mass more than m_Z then only the other one can contribute to the Bjorken process. The results in this case, for the same representative values of $\tan\beta$, namely 1 (solid line), and 10 (dashed line), are shown in fig. 4. The allowed masses and mixing angles are to the right of the curves. When H_2 is the lighter scalar, the mass bound must reduce to the SM value in the $\theta = 90^o$ limit, independent of $\tan\beta$, in consonance with eq. (4). (If H_1 is the lighter one, then the corresponding limit is $\theta = 0^o$.) Our findings agree with that of the L3 group [1] who obtain a bound of 58 GeV for the SM Higgs using only the invisible decay modes. They also quote a stronger bound of 60.2 GeV, but this utilises other Z-decays (*e.g.* to charged leptons) as well, and consequently is not of relevance to this discussion. Notice that depending on the mixing angle, in this model a light scalar is still allowed by the data. We have checked that these limits are insensitive to the mass of the heavier scalar.

With a larger integrated luminosity available, for the same choice of parameters the bounds are now strengthened compared to earlier work [11]. In this analysis, for the $x \neq 0$ case, the mixing angle θ can be zero only if $\xi = 0$ – see eq. (5). In this limit the state H_1 is purely doublet and also has no coupling to JJ, independent of $\tan\beta$. This is borne out in Fig. 4 by the coming together of the curves for different $\tan\beta$ in this limit. Near $\theta = 0$, the state H_2 is almost purely singlet – at $\theta = 0$ this scalar cannot be produced in the Bjorken process at all – and its decay to the invisible JJ final state is controlled by the product $\lambda' x$ – see eq. (10) – which is inversely proportional to x (note eq. (7)). Consequently, for small θ the bound on H_2 in fig. 4 is weakened for larger $\tan\beta$. The $\theta = \pi/2$ case is very similar except that H_1 and H_2 are interchanged.

5 PRODUCTION AND DETECTION AT THE LHC

Now we turn to the production and detection possibilities of the scalars of this model at hadron colliders, specifically the LHC.

For the $x = 0$ case, there is no mixing between the doublet and the singlet scalars. The production from gluon fusion remaining unchanged, the only difference from the SM will be in the branching ratios of the Higgs scalar since new decay modes become available. All SM decay channels suffer the same suppression in the BR due to the

additional invisible modes discussed in section 3. This suppression ratio has been plotted in fig. 2. Thus, if an SM-like Higgs is observed at the LHC with the ratio of BRs consistent with the Standard Model but the apparent production rate smaller than expected, then that could be indicative of this scenario.

The $x \neq 0$ case has more novelty. Like the SM Higgs, H_1 and H_2 can be produced at the LHC by gluon-gluon fusion [12]. The production rate is suppressed with respect to the SM case by appropriate mixing angle factors. Our stress will be on the production of the heavier one, which we term H, and its subsequent decay to a pair of the lighter – h – ones [13]. This decay mode, if kinematically allowed, can give rise to new signals. We look for both the hs decaying to $b\bar{b}$ giving rise to $4b$ final states or one of the hs decaying to $b\bar{b}$ and the other to a pair of Js, yielding missing E_T plus $2b$ final states.

Unfortunately, both channels, though somewhat novel, suffer from large QCD backgrounds. The potential source of background to the first channel is (a) QCD $4b$ production and (b) pair production of Z^0s both of which decay in the $b\bar{b}$ mode. The latter is removed by the invariant mass cut imposed on the b-pairs (see below). A further contribution comes from $b\bar{b}gg$ production where the gluon jets are misidentified as b-jets. The main background for the other channel comes from the QCD 3 jet ($b\bar{b}g$) process, where the gluon jet is outside the rapidity coverage of the detector and gives rise to missing E_T. We have analysed these backgrounds with parton-level Monte Carlo generators.

Before delving into the details of the analysis of the signals (and the backgrounds) let us pay some attention to the relevant branching ratios of interest, namely BR ($H \to b\bar{b}$), BR ($H \to hh$), and, finally, BR ($H \to JJ$). Some representative results are shown in figs. 5 and 6 where m_h is fixed at 70 GeV. The convention is as follows:
solid line : $H \to b\ \bar{b}$
large-dashed line : $H \to hh$
small-dashed line : $H \to JJ$
For the purpose of illustration, results are presented for $\tan\beta = 1$ and $\tan\beta = 10$ and mixing angles $\theta = 5^o$ and 45^o. The results for $\theta = 85^o$ are almost identical to the $\theta = 5^o$ case under the interchange $H_1 \leftrightarrow H_2$. From the plots it is seen that for the two exhibited mixing angles the situations are vastly different and we now discuss them in turn.

First consider the case of $\theta = 5^o$ (fig. 5). For $H \equiv H_1$ the dominant decay mode is to a pair of bs. The 3 body decay $H \to WW^* \to Wf\bar{f}'$ which opens beyond the $Wf\bar{f}'$ threshold is also comparable but is not relevant for this work and has not been displayed. Beyond the W^+W^- threshold the other branching ratios are all very small. On the other hand, for $H \equiv H_2$, it is the invisible decay which is the dominant one.

For $\theta = 45^o$ (fig. 6) and $\tan\beta = 10$, the $H \to hh$ mode is dominant once it is kinematically allowed and the two cases $H \equiv H_1$ and $H \equiv H_2$ are almost identical. The $\tan\beta = 1$ and $H \equiv H_2$ case is unusual in that the Hhh coupling vanishes identically. This is not so for $H \equiv H_1$.
We have not shown the branching ratios of $h \to b\,\bar{b}$ and $h \to JJ$. We have checked that these BRs are independent of m_H. This allows us to use the following approximate prescription:

$$\mathrm{BR}(h \to JJ)_{(\theta, m_h = 70\mathrm{GeV})} = \mathrm{BR}(H \to JJ)_{(\frac{\pi}{2} - \theta, m_H = 70\mathrm{GeV})}$$

and an analogous one for the $b\bar{b}$ mode. The branching ratios for h can then be read off from figs. 5 and 6 from the extremal points $m_H = m_h = 70$ GeV.
We now turn to the detection possibilities. First, we look at the $4b$ final state which has also been examined in the context of supersymmetric Higgs boson search [14]. This mode suffers from a huge QCD background. We have analysed both the signal and the background at the parton level using a Monte Carlo event generator. The MRSA parton distribution functions [15] have been used. Signal events consist of 4 hard b-jets. We have incorporated a QCD enhancement factor ($\simeq 1.5$) [16] for the calculation of the signal. Conservatively, we assume the b-tagging efficiency is on the average equal to 30% [17]. The main background is due to the QCD $4b$ process. An additional contribution comes from QCD $b\bar{b}gg$ production, where the gluon jets are mis-tagged as b-jets. We did not analyse this latter process separately, but assume that it contributes as much as the $4b$ background itself – a very safe estimate. The final state particles being almost massless with respect to the LHC center of mass energy, the jets are boosted in the forward direction both for the signal and the background. The following cuts are imposed in line with the LHC detectors:

p_T of each jet is greater than 15 GeV.

$|\eta|$ of each jet is less than 2.5

The kinematic distribution of the signal and the background events are similar and the cuts are not of much help in boosting their ratio. The main difference between them is that for the former the jets are due to the two body decay of the scalars of lighter mass, which, in turn, are pair produced when the heavier scalar decays. This is incorporated in the analysis by demanding that in addition to the constancy of the $4b$ invariant mass, it should be possible to combine the b-jets into two pairs of the same invariant mass.
In fig. 7 the variation of the Significance ($= \frac{S}{\sqrt{B}}$) with the 4-jet invariant mass – m_H – is exhibited for different values of the di-jet invariant mass – m_h. We present the

results for $m_h = 70$ (7a), 100 (7b) and 130 GeV (7c). The proposed LHC integrated luminosity of $10^5 pb^{-1}$ for a one year run – the high luminosity option – has been used. Results for $\tan\beta = 10$ and 1 are shown and θ has been chosen to be 45^o.
For $\theta = 5^o$ the Significance is much smaller. This can be traced to the following: If $H \equiv H_1$ – predominantly the doublet scalar – the small mixing angle suppresses the decay $h \to b\bar{b}$ while for $H \equiv H_2$ – essentially a singlet scalar – the production of H is very small for the same reason. In addition, there is a further reduction due to the smallness of the $H \to hh$ branching ratio in this case.
The notation in fig. 7 is as follows: $\tan\beta = 10$ for the solid and large dashed lines which correspond to $H \equiv H_1$ and $H \equiv H_2$ respectively. The small-dashed line is for $H \equiv H_1$ and $\tan\beta = 1$. (The case $H \equiv H_2$ and $\tan\beta = 1$ does not provide a signal, see below.) From fig. 7a it is seen that so long as the 4-jet invariant mass is less than twice the W mass the magnitude of the Significance is experimentally viable. But once the WW threshold is crossed, the Significance comes down even below unity. This reflects the fact, mentioned earlier, that if the WW decay is kinematically allowed, it dominates over the other modes. The number of $4b$ events from the background is also very high in this region. As the 4-jet invariant mass is increased, the number of background events drops sharply. So for higher values of the 4-jet invariant mass – see also figs. 7b and c – the Significance again climbs up. At first sight, it may seem odd that the Significance increases with m_H. This is actually due to the rapid fall in the background, which more than compensates the gentle decrease of the signal. Notice that we do not present any results for the $\tan\beta$ =1 and $H \equiv H_2$ case. This is because, as noted earlier, for this case the $H \to hh$ decay is forbidden.
The Significance is seen to be higher for the $\tan\beta = 10$ case. The signal cross-section can be further increased by choosing a larger $\tan\beta$. But $\tan\beta$ beyond 10, pushes the singlet *vev*, x, beyond the TeV scale, which is not very appealing.
Next, consider the case when one of the h decays invisibly through the JJ mode leaving a 2 b-jets $+\not{E}_T$ signal. As pointed out earlier, the main source of background for this channel is the QCD $b\bar{b}g$ events when the gluon jet is outside the rapidity coverage of the detector. Another source of background is $b\bar{b}\nu\bar{\nu}$ production where the νs originate from the decay of a Z^0. But this latter rate is suppressed with respect to the previous one and is ignored. As can be seen from the branching ratio plots in figs. 5 and 6, for $\tan\beta = 1$ the branching ratio of the invisible decay of the lighter scalar becomes dominant over the $b\bar{b}$ decay in most cases. Thus the number of signal events for this final state for $\tan\beta = 1$ can be quite substantial. But the presence of a large amount of missing energy in the signal events undermines any mass reconstruction strategy similar to the one used for the $4b$ final state. In the absence of such a procedure the background overwhelms the signal and no further results are presented

for this decay channel.
We have not discussed the direct production and decay of the lighter scalar h so far. The production rate, *via* gluon fusion, will be suppressed compared to the SM rate by mixing angle factors. For the decays, in addition to the analogous mixing angle factor suppression, there will be a new invisible decay mode, namely $h \to JJ$. The resultant effect is summarised, for the case $h \equiv H_1$, in Table 1 where we list the ratio $r = \sigma(pp \to h + X \to b\bar{b} + X) \ / \ \sigma(pp \to h + X \to b\bar{b} + X)_{SM}$ for different m_h, θ and $\tan\beta$.

6 CONCLUSION

We examined the simplest extension of the SM, with an additional $SU(2) \times U(1)$ singlet scalar field. We separately considered the cases (a) the singlet has no *vev* and (b) the singlet has a non-vanishing *vev*. In the former case, there is no mixing of the doublet scalar field with the singlet field. The only difference from the SM arises from new decay modes of the doublet scalars to singlets via a quartic coupling term. In the latter case, there are two massive neutral scalar fields – linear combinations of the doublet and the singlet states – with non-vanishing coupling to the goldstone boson, J. We have updated the bounds on the masses of the scalars in both scenarios from the LEP-1 data.
Here, we have not considered the expectations from this model for LEP-2. In a recent paper [18] de Campos *et al.* consider the mass bounds that may be obtained from LEP-2 for an invisibly decaying scalar. Though their model is somewhat different (two doublets and one singlet) it reduces to the one of this paper in a suitable limit. We have checked, using a parton level Monte Carlo and imposing the appropriate cuts, that our results agree with theirs in this limit.
We have investigated the detection possibilities of the scalars at the LHC, especially for the $x \neq 0$ case, using parton-level Monte Carlo event generators. In our analysis we consider the heavier scalar decaying to a pair of the lighter ones, both of which subsequently decay either to $b\bar{b}$ yielding a $4b$ final state or one of the lighter scalars decays invisibly (*i.e.* to JJ), giving rise to a $2b + \not{E}_T$ signal. Both the channels suffer from large QCD backgrounds which have also been examined. Using a mass reconstruction strategy for the $4b$ final state we observe that for some regions of the parameter space these scalars are likely to be seen at the LHC.

Acknowledgements

AR acknowledges partial financial support from the Council of Scientific and Industrial Research and the Department of Science and Technology, Government of India. Both authors are grateful to Biswarup Mukhopadhyaya for participation in the initial stages of the work. They acknowledge fruitful discussions with Gautam Bhattacharyya.

References

[1] *The L3 Collaboration*, *Phys. Lett.* **B385**, 454 (1996).

[2] Among the other LEP experiments, ALEPH obtains a bound of 63.9 GeV for the SM Higgs mass using both invisible and charged leptonic modes in the Bjorken process. From only the former, their limit is 62.9 GeV. *The ALEPH Collaboration*, *Phys. Lett.* **B384**, 427 (1996); The corresponding results from OPAL are 60.6 GeV and 59.6 GeV respectively. *The OPAL Collaboration*, *Z. Phys.* **C73**, 189 (1997).

[3] For the first results from LEP-2, see *The ALEPH Collaboration*, CERN Report, CERN PPE-97-070 where a bound on the SM Higgs mass of 69.4 GeV is obtained; OPAL quotes a bound of 65.0 GeV. *The OPAL Collaboration*, *Phys. Lett.* **B393**, 231 (1997).

[4] J. Gunion, *et al.*, *The Higgs Hunter's Guide* (Addison Wesley Publishing Company, Menlo Park, 1991). For a detailed study of the detection possibilities of the MSSM Higgs at hadron colliders see Z. Kunszt and F. Zwirner, *Nucl. Phys.* **B385**, 3 (1992).

[5] F. Gürsey and P. Sikivie, *Phys. Rev. Lett.* **36**, 775 (1976); *Phys. Rev.* **D16**, 816 (1977); see also T. Rizzo and J.-A. Hewett, *Phys. Rep.* **183**, 193 (1989).

[6] J.C. Pati, *Phys. Lett.* **B228**, 228 (1989); K.S. Babu, J.C. Pati and H. Stremnitzer, *Phys. Rev.* **D51**, 2451 (1995) and references therein.

[7] J. Ellis, J.F. Gunion, H.E. Haber, L. Roszkowski and F. Zwirner, *Phys. Rev.* **D39**, 844 (1989).

[8] Y. Chikasige, R.N. Mohapatra and R.D. Peccei, *Phys. Lett.* **B98**, 265 (1980).

[9] A.S. Joshipura and S.D. Rindani, *Phys. Rev. Lett.* **69**, 3269 (1992).

[10] R.E. Schrock and M. Suzuki, *Phys. Lett.* **B10**, 250 (1982); L.F. Li, Y. Liu, and L. Wolfenstein, *ibid.* **B159**, 45 (1985); E.D. Carlson and L.J. Hall, *Phys. Rev.* **D40**, 3187 (1985); G. Jungman and M.A. Luty, *Nucl. Phys.* **B361**, 24 (1991); J.C. Romao, F. de Campos, and J.W.F. Valle, *Phys. Lett.* **B292**, 329 (1992).

[11] B. Brahmachari, A.S. Joshipura, S.D. Rindani, D.P. Roy, K. Sridhar, *Phys. Rev.* **D48**, 4224 (1993);

[12] V. Barger and R.J.N. Phillips, *Collider Physics*, (Addison-Wesley Publishing Company, Menlo Park, 1987).

[13] For search strategies at the LHC involving alternative modes which probe complementary regions of the parameter space, see D. Choudhury and D.P. Roy, *Phys. Lett.* **B322**, 368 (1994).

[14] J. Dai, J.F. Gunion, R.Vega, *Phys. Lett.* **B387**, 801 (1996).

[15] A.D. Martin, R.G. Roberts and W.J. Stirling, *Phys. Rev.* **D50**, 6734 (1994).

[16] M. Spira, A. Djouadi, D. Graudenz and P. Zerwas, *Nucl. Phys.* **B453**, 17 (1995).

[17] ATLAS Collaboration, W.W. Armstrong, *et al.*, Technical Proposal CERN/LHCC/94-43 (December 1994); CMS Collaboration, G.L. Bayatian *et al.*, Technical Proposal CERN/LHCC/94-38 (December 1994).

[18] F. de Campos, O.J.P. Eboli, J. Rosiek, J.W.F. Valle, *Phys. Rev.* **D55**, 1316 (1997)

FIGURE CAPTIONS

Fig.1. The number of events in the di-jet + $\not{E}$ channel of Z-decay as a function of m_H. The limit on m_H from non-observation of a signal corresponds to the intercept on the abscissa. The solid, large-dashed and small-dashed curves correspond to $\xi =$ 1, 0.0001 and 0 (SM) respectively. Two choices of m_N – 20 GeV (1a) and 0 GeV (1b) – are shown.

Fig. 2. The ratio $r = \mathrm{BR}(H \to \gamma\gamma)/\mathrm{BR}(H \to \gamma\gamma)_{SM}$ as a function of m_H for different values of ξ.

Fig. 3. The allowed mass ranges of the two scalars (to the right of the curves) for the case $x \neq 0$ when both are lighter than the Z-boson and can be produced *via* the Bjorken process. Results are shown for two values of $\tan\beta$: 1 (solid line), and 10 (dashed line). Three choices of θ – 5^o, 45^o, and 85^o – have been considered.

Fig. 4. The allowed mass ranges of the lighter scalar as a function of the mixing angle for the case $x \neq 0$ when the other scalar is heavier than the Z-boson. Results are shown for two values of $\tan\beta$: 1 (solid line), and 10 (dashed line). The allowed regions are to the right of the curves.

Fig. 5. Branching ratio of the heavier scalar, H, to decay to $b\bar{b}$ (solid line), JJ (small-dashed line), and hh (large-dashed line). The two possibilities $H \equiv H_1;\ h \equiv H_2$, and $H \equiv H_2;\ h \equiv H_1$, have been considered. The results for two choices of $\tan\beta = 1$ and 10 have been shown and the mixing angle θ is chosen to be 5^o.

Fig. 6. Same as in fig. 5 except that the mixing angle θ is 45^o.

Fig. 7. Significance $(S/\sqrt{B})$ as a function of m_H for three different choices of m_h – 70 GeV (a), 100 GeV (b), and 130 GeV (c). $\tan\beta = 10$ for the solid and large dashed lines which correspond to $H \equiv H_1$ and $H \equiv H_2$ respectively. The small-dashed line is for $H \equiv H_1$ and $\tan\beta = 1$.

TABLE CAPTION

Table 1: The ratio $r = \sigma(pp \to h + X \to b\bar{b} + X)\ /\ \sigma(pp \to h + X \to b\bar{b} + X)_{SM}$, for the case $h \equiv H_1$ for different values of m_h, $\tan\beta$ and θ.

Table 1

r				
		m_h		
θ	$\tan\beta$	70 GeV	100 GeV	130 GeV
5^o	1	.9624	.9344	.9151
	10	.9920	.9917	.9900
45^o	1	.0986	.0549	.0415
	10	.4804	.4609	.3830
85^o	1	1.427×10^{-5}	7.166×10^{-6}	5.27×10^{-6}
	10	.0012	.0006	.0002

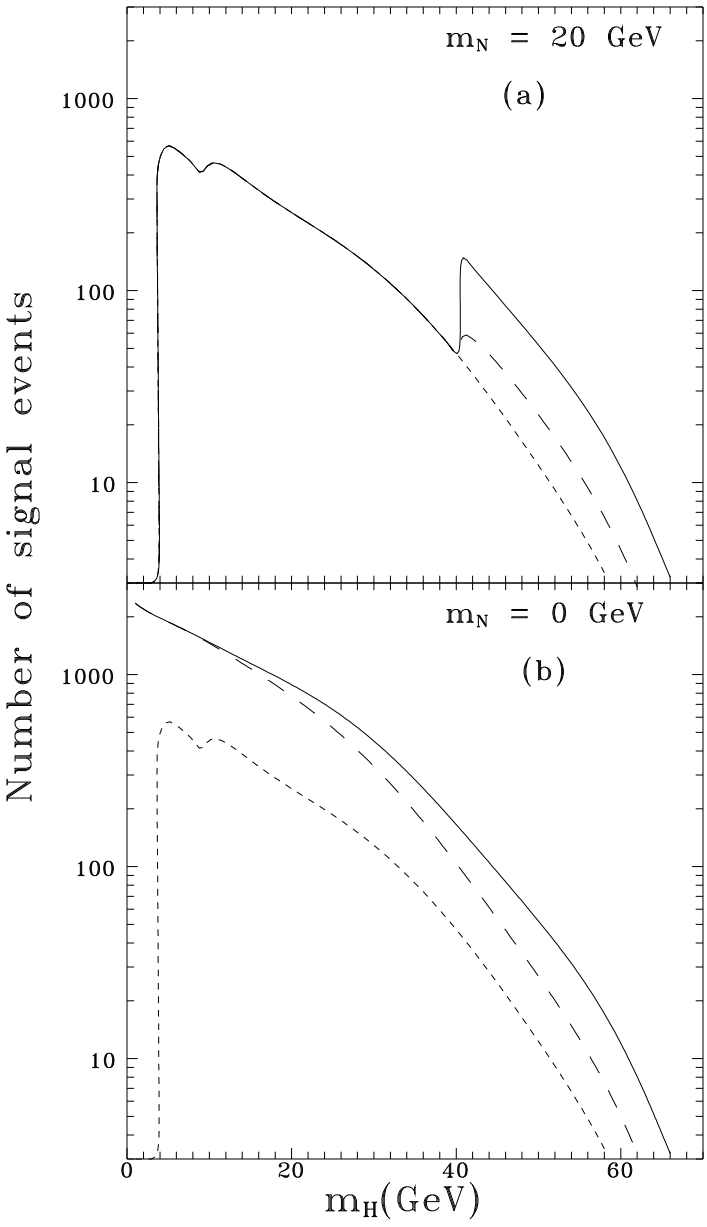
m_N = 20 GeV
(a)
1000
100
10
m_N = 0 GeV
(b)
1000
100
10
0
20
40
60
Number of signal events
m_H(GeV)
Fig. 1

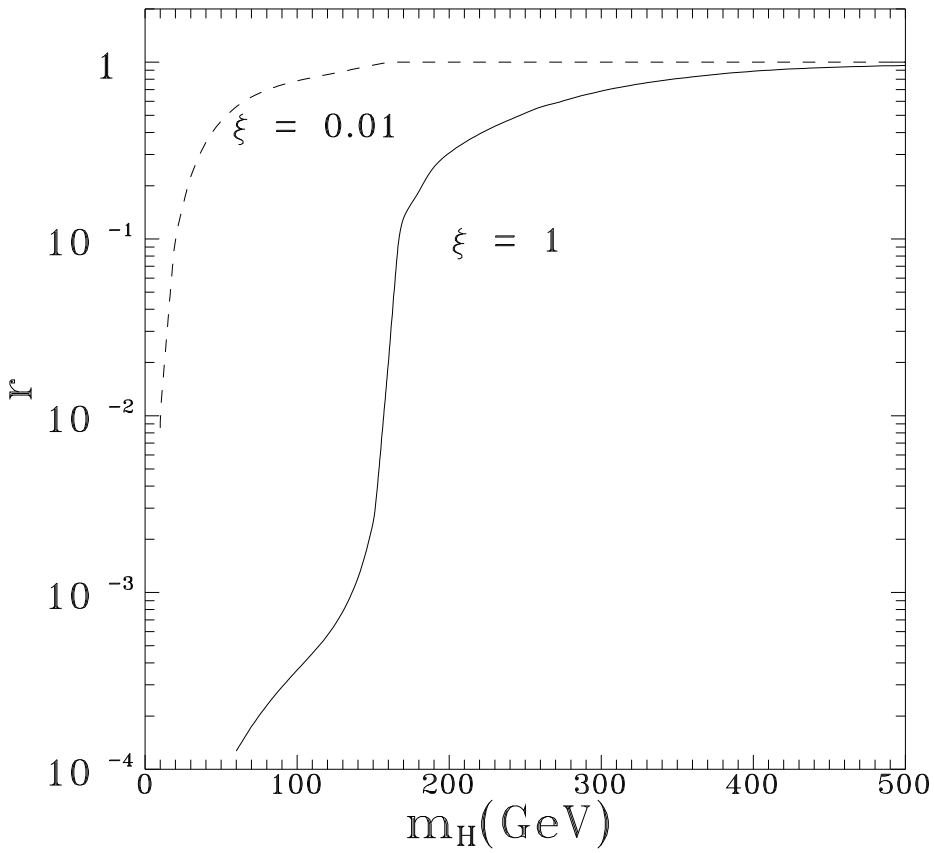

Fig. 2

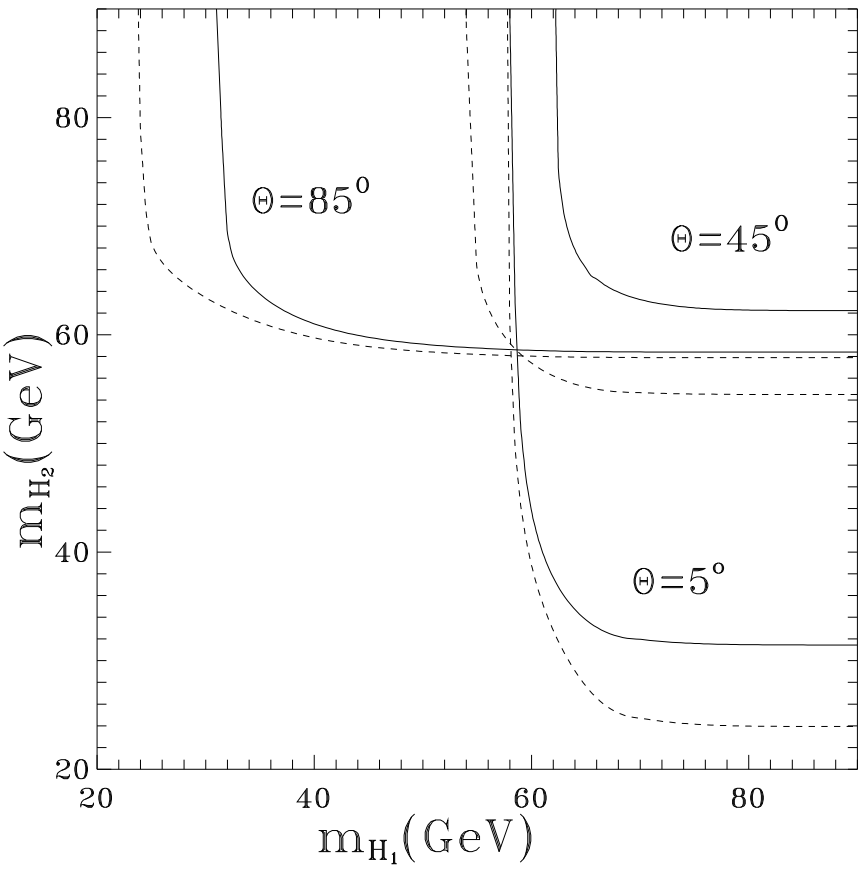
80
60
40
20
20
40
60
80
$\Theta=85^{o}$
$\Theta=45^{o}$
$\Theta=5^{o}$
$m_{H_2}(GeV)$
$m_{H_1}(GeV)$

Fig. 3

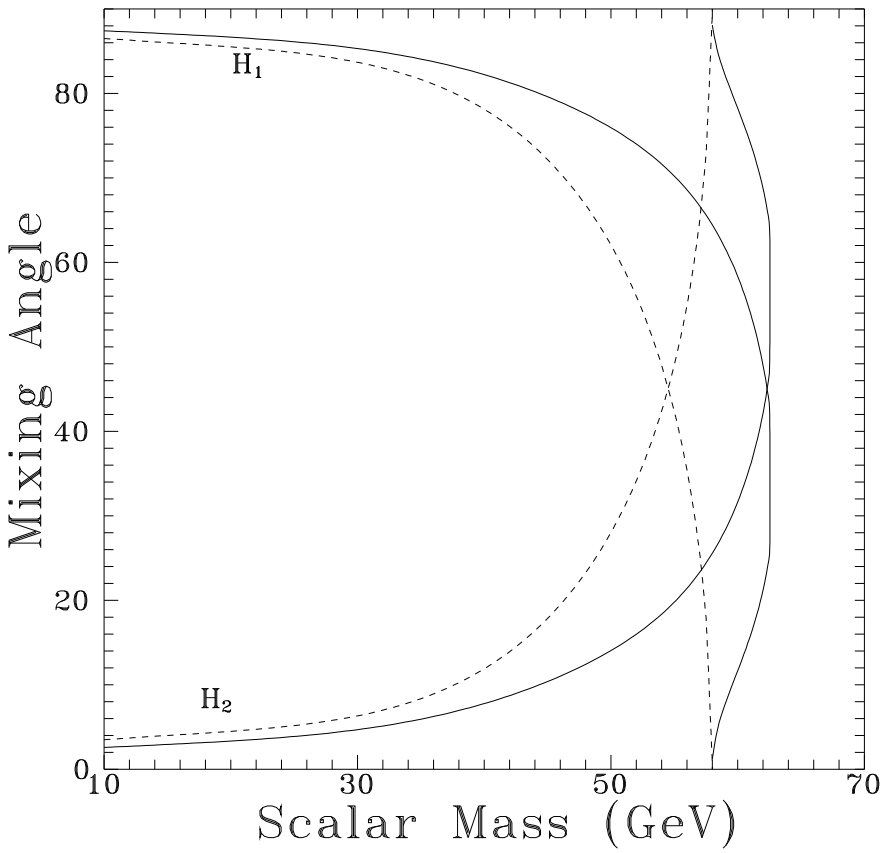

Fig. 4

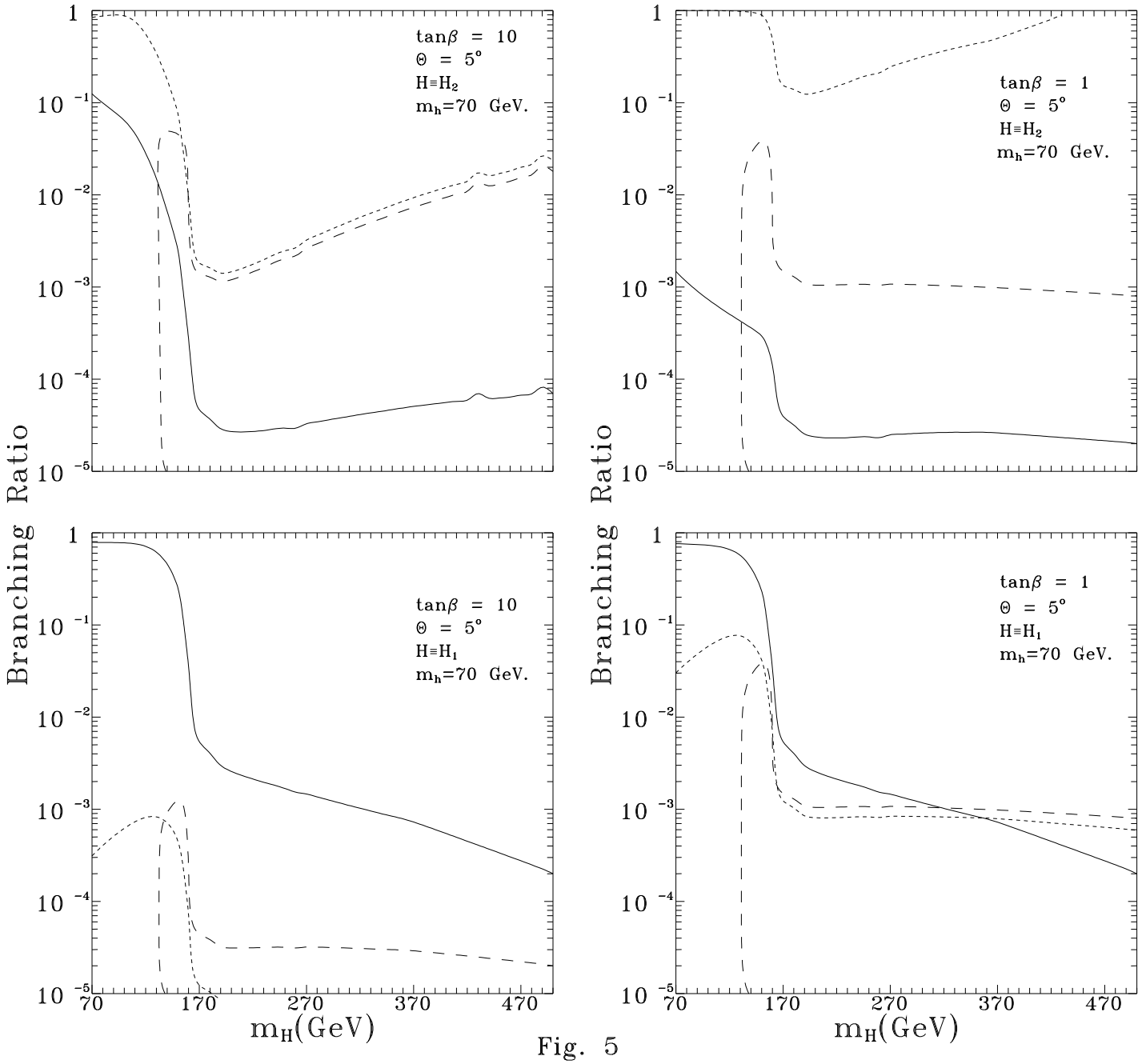
Branching Ratio
tanβ = 10
Θ = 5°
H≡H2
mh=70 GeV.
tanβ = 1
Θ = 5°
H≡H2
mh=70 GeV.
tanβ = 10
Θ = 5°
H≡H1
mh=70 GeV.
tanβ = 1
Θ = 5°
H≡H1
mh=70 GeV.
mH(GeV)
mH(GeV)

Fig. 5

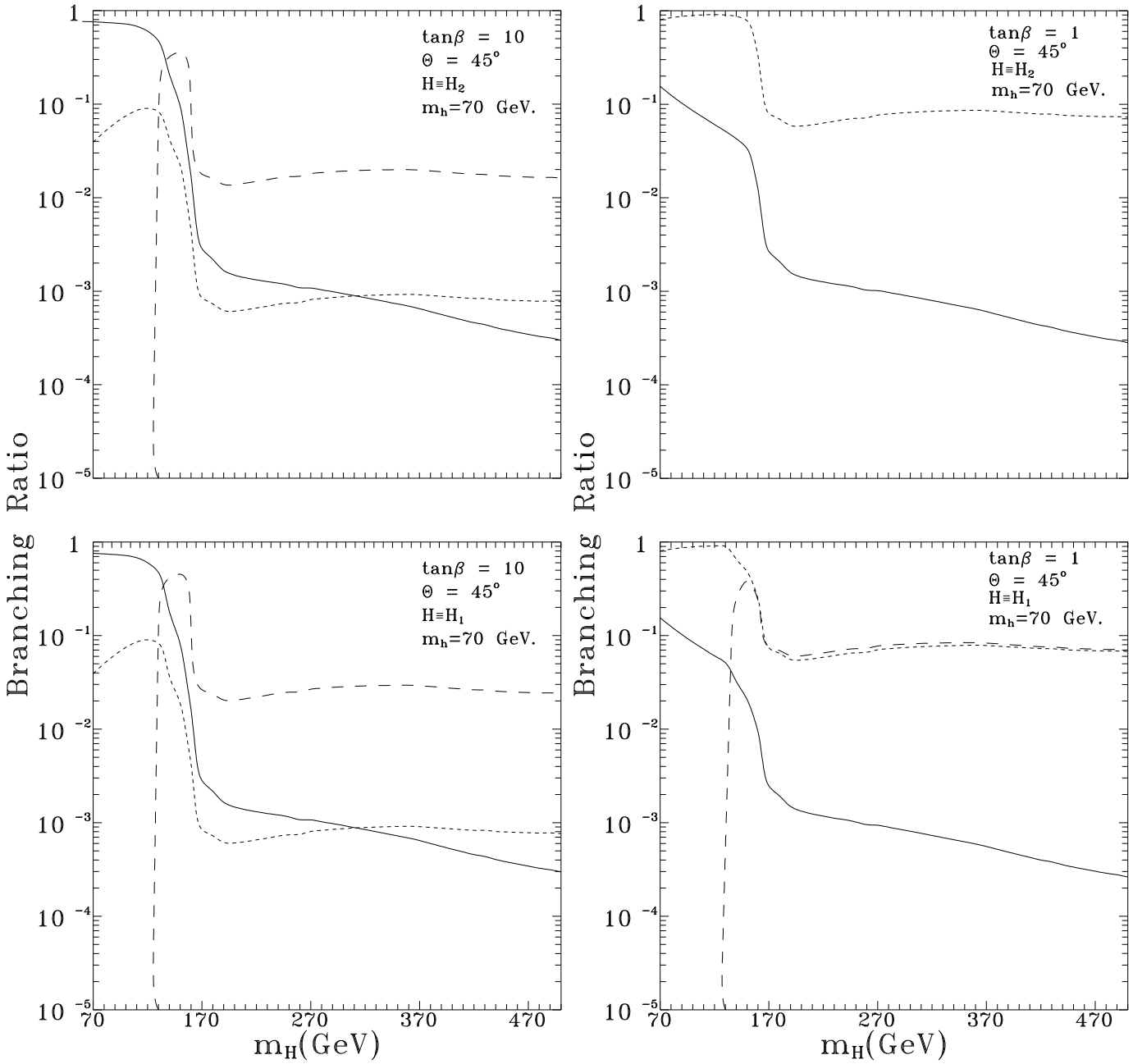
Branching Ratio
tanβ = 10
Θ = 45°
H≡H2
mh=70 GeV.
tanβ = 1
Θ = 45°
H≡H2
mh=70 GeV.
tanβ = 10
Θ = 45°
H≡H1
mh=70 GeV.
tanβ = 1
Θ = 45°
H≡H1
mh=70 GeV.
1
10 -1
10 -2
10 -3
10 -4
10 -5
70
170
270
370
470
mH(GeV)

Fig. 6

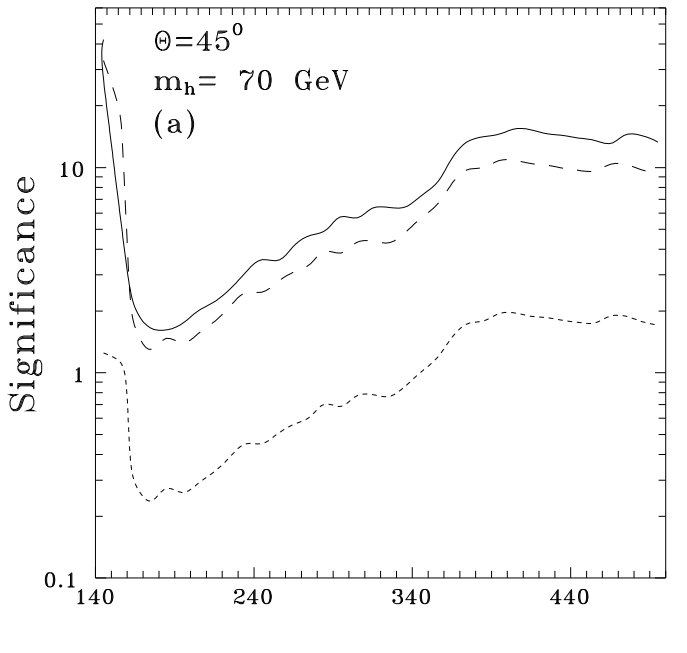
Θ=45°
m_h= 70 GeV
(a)
Significance
10
1
0.1
140
240
340
440

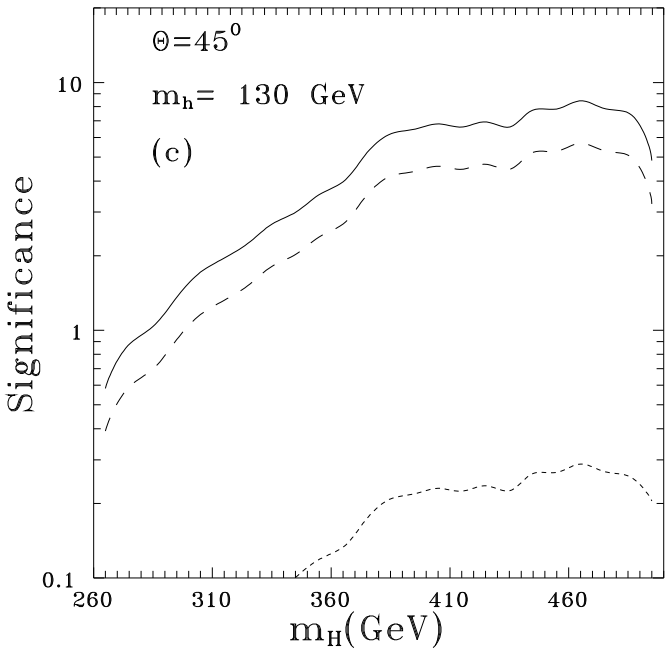
Θ=45°
m_h= 130 GeV
(c)
Significance
10
1
0.1
260
310
360
410
460
m_H(GeV)

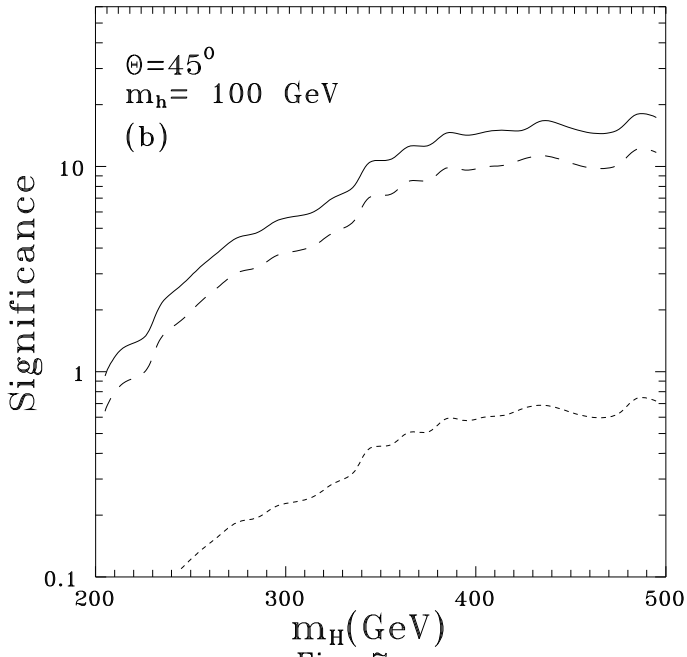
Θ=45°
m_h= 100 GeV
(b)
Significance
10
1
0.1
200
300
400
500
m_H(GeV)

Fig. 7